Development of Simulation Method for Multiphase Flows : Application to Gas-Liquid and Gas-Solid Two Phase Flows

Sumitomo Chemical Co., Ltd.
Process & Production Technology Center
Naoki SHIMADA
Tomonari KOBAYASHI
Tetsuya SUZUTA

We have several processes consisting of mixture of gas, liquid and solid, known as multiphase flow processes, in chemical engineering. In this paper, the simulation method used to deal with such processes in our company has been introduced. Following are examples of some applications, (1) Simulation of liquid mixing in a bubble column, (2) DEM-CFD coupling simulation for fluidized bed with small particles, (3) Simulation of single bubble and droplet by using interface tracking type method.

This paper is translated from R&D Report, "SUMITOMO KAGAKU", vol. 2012.

Introduction

A variety of processes (multiphase flow processes) that mix and move gases, liquids and solids are used in chemical engineering. Bubble columns and fluidized beds are multiphase flow apparatuses that have been known for a long time. Examples to these apparatuses are shown in **Fig. 1**.[1)]

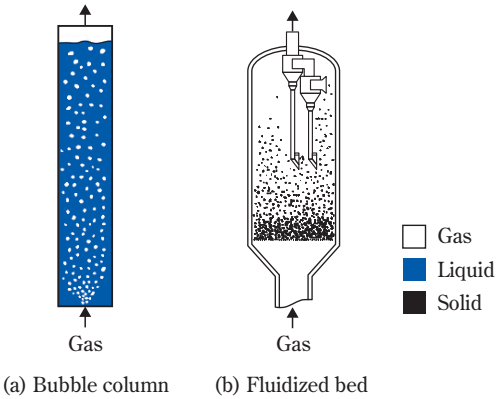

Fig. 1 Multiphase flow reactors[1)]

Multiphase flows encompass wide-ranging scales and a variety of phenomena, and there are many engineering problems that should be solved remaining. Approaches from a variety of points of view are actively being pursued to move this field forward. Simulation techniques are no exception. By getting a good understanding of, verifying and skillfully using data that is captured, we can expect powerful designs and rationalized support techniques for chemical engineering.

Fig. 2 shows research classified according to the type of numerical solution. Taking a lesson from the classifications of Tomiyama,[2)] numerical solutions for multiphase flows were divided into (1) interface tracking models, (2) particle tracking models and (3) averaging models. (1) is methods that can capture the shape at

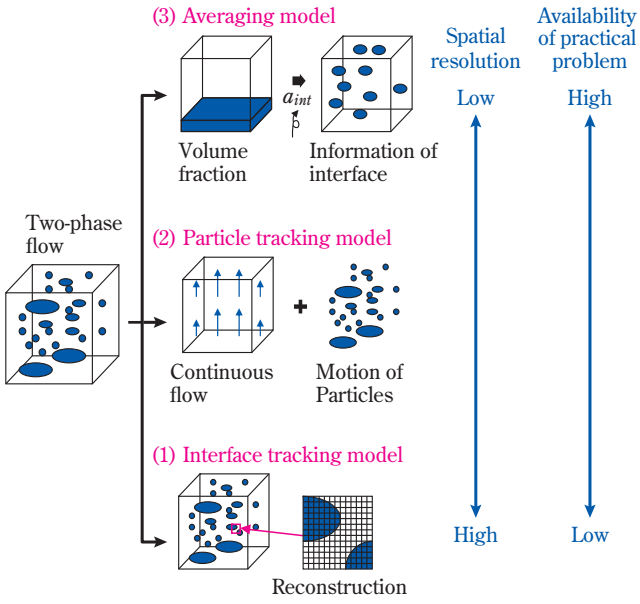

Fig. 2 Classification of computational multiphase fluid dynamics

interfaces that divide phases. (2) is methods for individually tracking constant shapes such as dispersed bubbles, droplets and particles while they are unchanged, and (3) is methods for calculating average values (for example, volume fraction and number density) for phases. Moving from (1) to (3), the flow becomes coarser grained, but in compensation for that applicability to practical problems increases. Also, there are a large number of methods such as the lattice Boltzmann method, particle method and boundary fitted coordinate method, but these will be omitted here in consideration of space.

In this article we will introduce multiphase flow simulation techniques the authors have been working on. For examples, we will specifically introduce simulations of liquid mixing properties in bubble columns, DEM-CFD coupling simulations for microparticle fluidized beds (discrete-element method (DEM) and computational fluid dynamics (CFD), one type of particle tracking model) and simulations using interface tracking models.

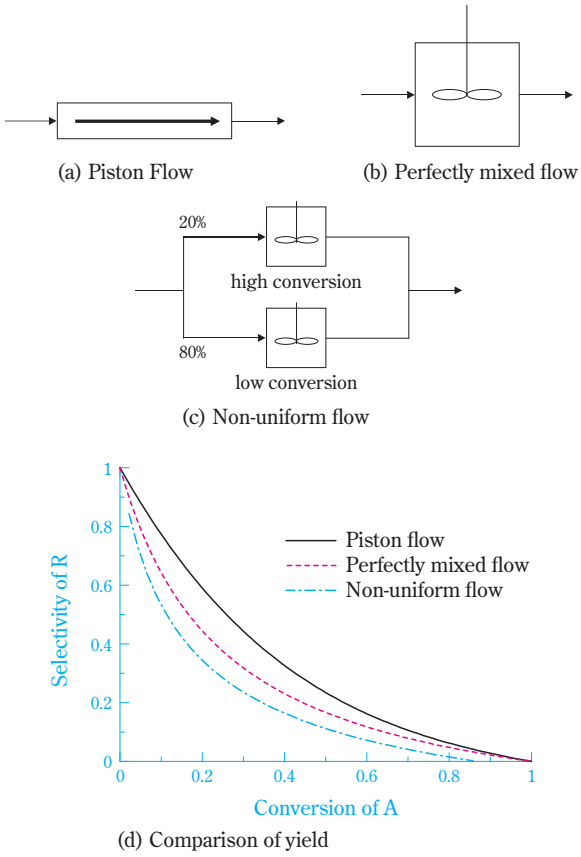

Fig. 3 Effect of liquid mixing on a reaction[3)]

Multiphase Flow Simulations

1. Simulations of Liquid Mixing Properties in Bubble Columns[3)]

The demand by enterprises for averaging and other models that easily handle large-scale industrial problems tends to remain high. This model finds an averaged phase volume fraction or number density using a fundamental equation with any of a statistic, time or space. Therefore, interface information (force applied to bubbles) that is lost by averaging must be supplied in the form of constitutive equations and correlations.

The flow and mixing properties of a substance can influence reactions. For example, consider a successive reaction (A → R → S) of three substances. **Fig. 3** shows an example of reaction computations. Considering a piston flow (**Fig. 3** (a), flow completely without back mixing), perfectly mixed flow (**Fig. 3** (b)) and non-uniform flow (**Fig. 3** (c)), the relationship between the reaction rate of substance A and selectivity of R are compared in **Fig. 3** (d). In these computations, it is assumed that a non-uniform flow has a flow divided 20% and 80%, with the former region reacting faster than the other region. From this comparison, it can be understood that the selectivity drops in the order of piston flow, perfectly mixed flow and non-uniform flow even if the reaction rate is the same.

If an averaging model is used, it is possible to efficiently understand how the liquid is mixed in the bubble column as a whole. Thus, we first verified the extent to which the model could predict the mixing properties of the liquid.

The mixing properties for the liquid were verified using the two types of apparatus shown in **Fig. 4**. One uses a perforated plate and the other uses a ring sparger to supply bubbles to the liquid. Tap water was used for the fluid with air. Measurement of mixing properties was carried out using a tracer method. After the gas-liquid flow reached a quasi-steady state, a red colorant and table salt were introduced stepwise through the liquid inlet, and the changes over time at the outlet were examined. **Fig. 5** shows an example of the results of visualization and measurements of the changes in outlet salinity C over time. The mixing coefficient E_L was found from these measured values using the following equation.

$$\frac{\partial C}{\partial t} + U_L \frac{\partial C}{\partial z} = E_L \frac{\partial^2 C}{\partial z^2} \quad (1)$$

Here, t is time, U_L the superficial velocity of the liquid in the column and z the distance for the height.

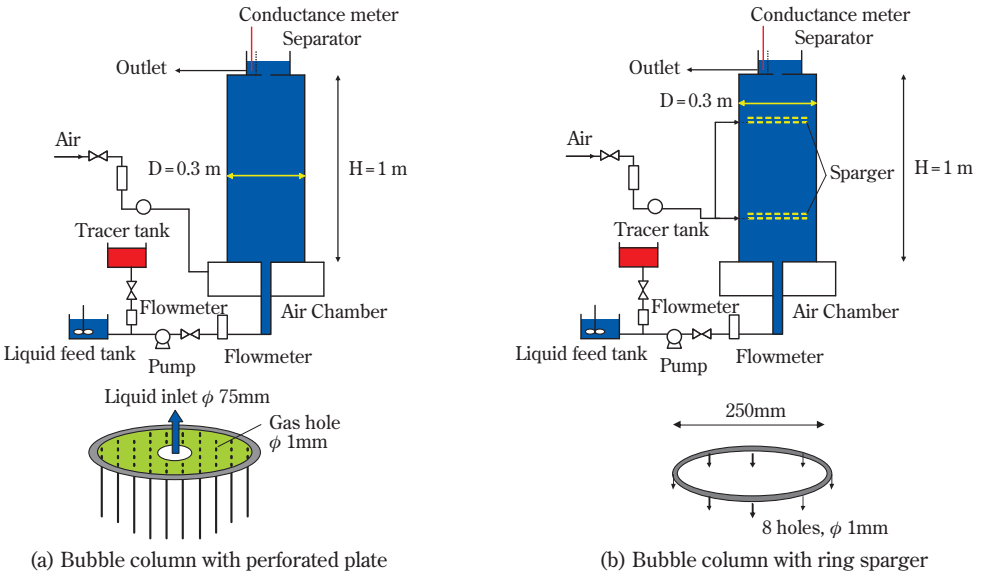

(a) Bubble column with perforated plate

(b) Bubble column with ring sparger

Fig. 4 Schematic of apparatus[3)]

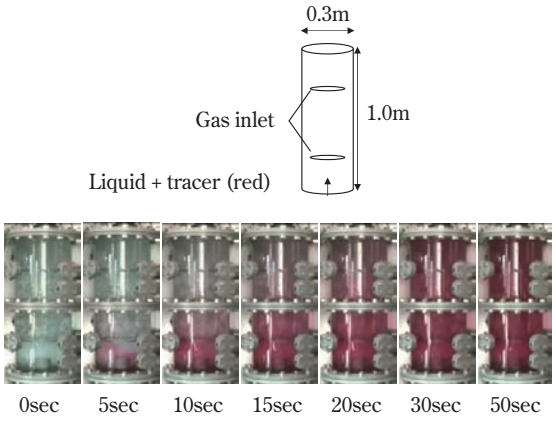

(a) Mixing process of tracers (red-colored)

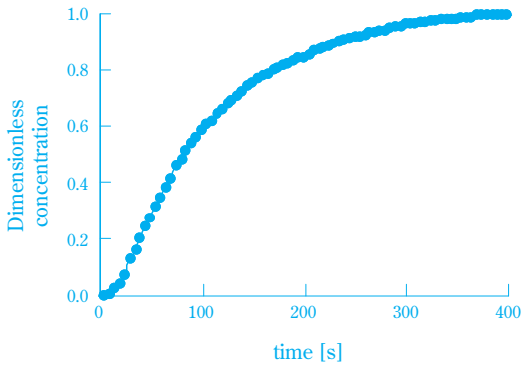

(b) Transient pattern of salinity at the outlet of the column (Concentration is normalized using steady-state value)

Fig. 5 Example of experiments using tracer method[3)]

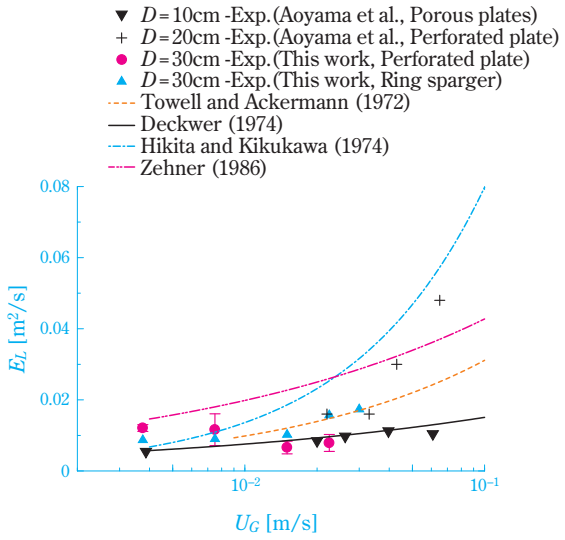

Fig. 6 Comparison of E_L[3)]

E_L was compared with values in references to confirm the reliability of the measurement results. The results are shown in **Fig. 6**. In these experiments, an approximately 20% repeatability error was confirmed. It was seen that this was the range of differences presented in the references by others.

These measurement results were compared with the results calculated by an (N+2)-field model (NP2 model). In consideration of space here, the details of the NP2 model are left to the references. The results are shown in **Fig. 7**. **Fig. 7** (a) is the effects of the gas superficial velocity on E_L, and **Fig. 7** (b) compares the effects of gas flow rate γ shown by the following equation on E_L.

$$\gamma = \frac{Q_{upper}}{Q_{upper} + Q_{lower}} \quad (2)$$

Here, Q_{upper} and Q_{lower} indicate the sparger flow rates set in the upper part and lower part, respectively. As can

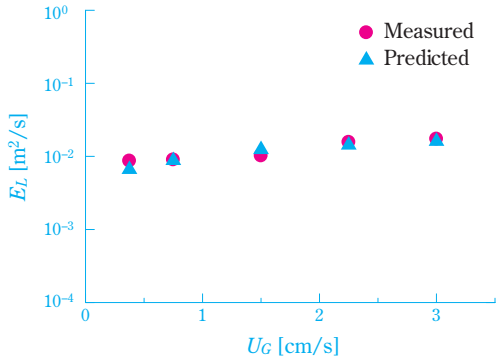

(a) Effect of U_G

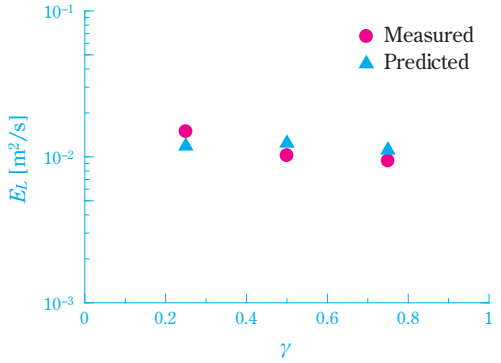

(b) Effect of ratio of upper to total gas flow rate γ

Fig. 7 Comparison between simulation and measurement[3)]

be seen from the results of the comparison, the calculations agree well with experimental values.

2. DEM-CFD Coupling Simulation for Microparticle Fluidized Bed[4)]

Next, we will introduce an example of work on an application of DEM-CFD coupling simulations. DEM-CFD coupling simulations are a computation method that couples the discrete element method (DEM) and computational fluid dynamics (CFD). DEM is a method that traces the movement of individual particles. The movement is taken as following Newton's equation of motion ($\boldsymbol{F} = m\boldsymbol{a}$, $\boldsymbol{F}$ being the force vector, m the mass and $\boldsymbol{a}$ the acceleration vector). At this time, the force used on each particle must be calculated to obtain accurate particle group behavior. The DEM used by the authors calculates the force $\boldsymbol{F}_i$ acting on the i^{th} particle by the following equation.

$$\boldsymbol{F}_i = \boldsymbol{F}_G + \boldsymbol{F}_C + \boldsymbol{F}_D + \boldsymbol{F}_{AD} \tag{3}$$

Here, $\boldsymbol{F}_G$ is gravity, $\boldsymbol{F}_C$ the contact force between particles, $\boldsymbol{F}_D$ the force received by the fluid and $\boldsymbol{F}_{AD}$ the adhesion force. A Voigt model formed by a spring-dashpot is typically used for $\boldsymbol{F}_C$. In most cases, particles are assumed to be spherical and not to deform so as to make the calculations of contact distance simple. A constant k, which indicates the strength of the spring, is an important parameter. When a linear spring model is used, $\boldsymbol{F}_C$ is given by the following equation.

$$\boldsymbol{F}_C = -kx - \eta\dot{x} \tag{4}$$

Here, x is the particle contact distance, and η is the coefficient of friction. $\boldsymbol{F}_D$ is calculated using the velocity of the fluid. Here, the velocity is found by CFD. A variety of forces that are used when detachment of particles from a state of contact can be considered for $\boldsymbol{F}_{AD}$. Here, a van der Waals force is assumed.

Evaluation of the contact state of particles through equation (3) is extremely important for performing calculations where particles are whirled up by gas being blown upward from the lower part as in a fluidized bed. In other words, consideration of the balance of forces among particles, whether the contact among the particles is not maintained such that gas flows between the particles and the particles move in a complex manner, or whether the particles maintain a state of contact, has a large effect. For example, of the balances described above, k, which shows repulsion, and $\boldsymbol{F}_{AD}$, which can inhibit this, are important.

Conversely, most research[4)] up to now has not viewed k as particularly important. This is because, in cases of particles where $\boldsymbol{F}_{AD}$ has almost no effect (for example, large particles with diameters of 1 mm or greater), the value of k has been found to have almost no effect on the fluidity of the particles. **Fig. 8** (a) shows a schematic diagram of the apparatus used, and **Fig. 8** (b) shows an example of the results of computations when $\boldsymbol{F}_{AD} = 0$. The black point groups show the particles, and the white parts show the gas phase. From **Fig. 8** (b), it can be seen that even if k changes 1000 fold, the particles are almost unaffected. If k becomes large, the repulsive force increases; therefore, the time for collisions arising at one time decreases. Therefore, the time steps for computations become shorter as k becomes larger, and longer computations must be carried out. In such circumstances, most calculations are done with k made as small as possible.

However, when particles on which $\boldsymbol{F}_{AD}$ acts (for example, particles classified in Geldart's group A, such

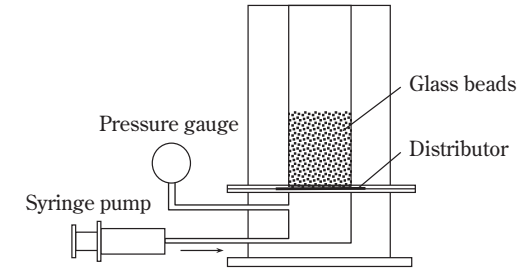

(a) Schematic of apparatus

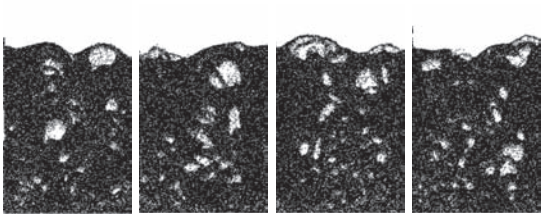

k=10 N/m　100 N/m　1×10³ N/m　1×10⁴ N/m

(b) without adhesion force

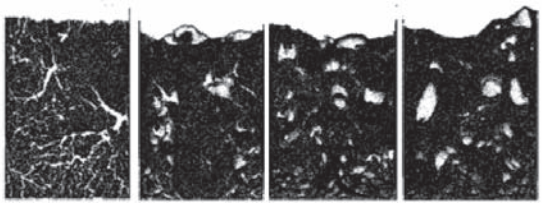

k=10 N/m　100 N/m　1×10³ N/m　1×10⁴ N/m

(c) with adhesion force

Fig. 8 Effect of k on fluidized behavior [4)]

as industrial catalysts) are used, the circumstances change. **Fig. 8** (c) shows a computation example when there is a value for $\boldsymbol{F}_{AD}$. It can be seen that smaller k becomes, the greater the influence of $\boldsymbol{F}_{AD}$ is and lower the fluidity of the particles is. **Fig. 9** shows the results of measurements of adhesive force on glass beads with a diameter of 60 μm. Particles with a diameter in this neighborhood are industrially important ones that are most frequently seen in catalysts and products.

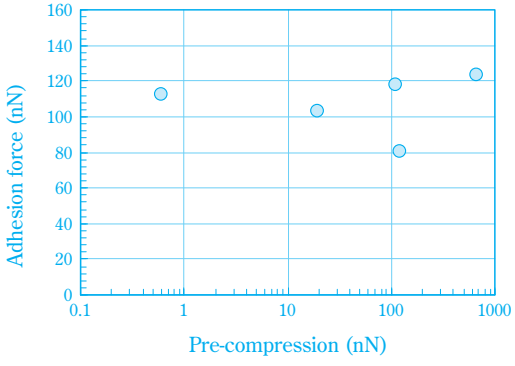

Fig. 9 Measurement of adhesion force [4)]

$\boldsymbol{F}_{AD}$ is approximately 100 nN, and this is a large value corresponding to approximately 40 times the weight of the particles. It cannot be made 0. From these results, it can be seen that (1) $\boldsymbol{F}_{AD}$ cannot be ignored in equation (3) and that (2) the fluidized behavior of the particles cannot be predicted unless a value is given to k that takes into consideration the balance with $\boldsymbol{F}_{AD}$.

Thus, the authors have proposed carrying out a dynamic analysis during the time a particle is in contact with a wall or another particle and finding k and $\boldsymbol{F}_{AD}$, then integrating this into a DEM-CFD coupling simulation.[4)] Specifically, as is shown in **Figs. 10** and **11**, the relationship with k and $\boldsymbol{F}_{AD}$ at the boundary line between the particle being repulsed and deflected (rebound state) and maintaining contact (sticking state) because of $\boldsymbol{F}_{AD}$ when in contact was examined. This is called a dynamic adhesion model. Please refer to our

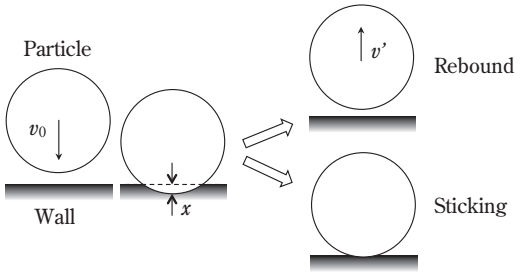

Fig. 10 Stick/rebound behavior after particle-wall collision [4)]

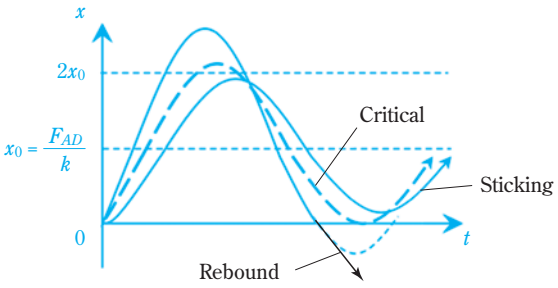

Fig. 11 Particle-wall overlaps in the duration of collision [4)]

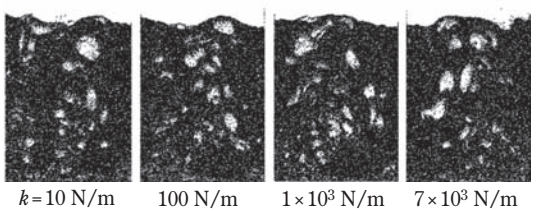

k=10 N/m　100 N/m　1×10³ N/m　7×10³ N/m

Fig. 12 Simulation with dynamic adhesion force [4)]

publication[4] for the details of the equations for the model. **Fig. 12** shows computational results when this model is used. From this figure, it can be seen that, even with small particles (catalysts and powders) for which adhesive force must be considered, bubble fluidization can be calculated independently of k. Moreover, computational results using k = 10 N/m use a larger time step then those using k = 7000 N/m ; therefore, an approximately sevenfold improvement in computation speed was confirmed.

3. Simulations Using Interface Tracking Model[5]

Last, we will introduce an example of interface tracking model. In this method up to now, computation load and constraints on computation time have been a problem, but with the dramatic developments in computer power in recent years, the advantage of being able to grasp the details of phenomena is being demonstrated. A variety of methods,[6] such as front tracking, level set and boundary fitting coordinates have been proposed for interface tracking models, but the authors tested the application of the following volume tracking method.

When it is assumed that both of two phases are incompressible flows and that substances do not include phase changes, the phase index α (for example, spatial average volume fraction, $0 \le \alpha \le 1$) is transported by the following equation.

$$\frac{\partial \alpha}{\partial t} + \boldsymbol{V} \cdot \nabla \alpha = 0 \qquad (5)$$

Here, t is time and $\boldsymbol{V}$ is fluid velocity. The second term on the left-hand side of this equation represents the convection item for α according to $\boldsymbol{V}$, but the following conditions must be satisfied.

(1) No numerical diffusion. The α of the α spatial derivative signifies the phase interface. In most cases, the interface has almost no thickness; therefore, α must diffuse with time.

(2) The numerical distribution for α must not overshoot or undershoot. In other words, α which signifies the volume fraction cannot be outside of the range of $0 \le \alpha \le 1$.

(3) Satisfies preservation of volume. In other words, when there is no entrance and exit of α in space θ, $\int_\theta \alpha d\theta$ must be constant.

(4) Even in multi-dimensions, the shape must be transported accurately.

As a method for equation (5) satisfying these, the authors focused on the tangent of hyperbola interface capturing (THINC) of Xiao et al.[7] It was possible to confirm that this method substantially satisfies (1)–(3) above. However, there was a problem with satisfying (4) above. Therefore, a function for optimizing the THINC parameters according to the orientation of the interface was added, and a new method was developed.[5] This method is called tangent of hyperbola for adaptive interface capturing (THAINC).

Fig. 13 shows an example of computations using THAINC. In the process of a single bubble rising, a substance O is dissolved in the liquid from the bubble. Furthermore, the O that is dissolved reacts with substance A in the liquid and produces product R, and product R reacts with O and produces byproduct S. The colors in

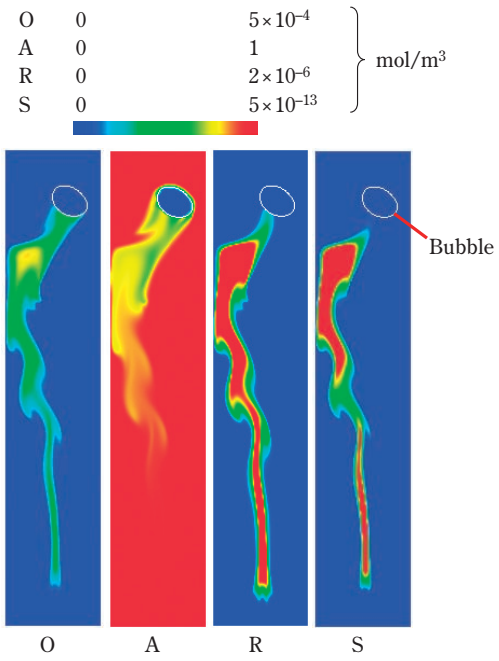

Fig. 13 Simulation of dissolution and reaction process with a single bubble [5]

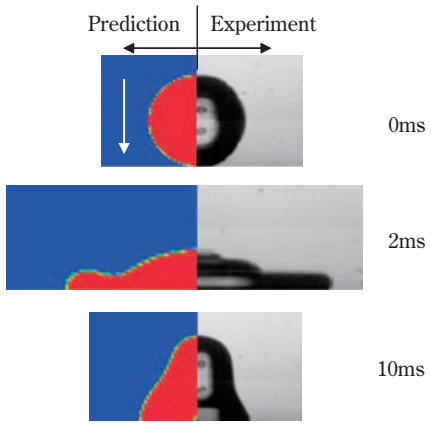

Fig. 14 Simulation of droplet deposition (Experiment by literature 8) [5]

the figure represent the concentration of each substance. An upward flow is created in the liquid with the rising of the bubble; therefore, it can be seen that a spatial distribution arises for each concentration.

This method can be developed for other systems such as droplets. **Fig. 14** is an example of computations for droplets. An experiment[8] is shown for comparison. It can be seen that computations can be done for a free falling droplet colliding with a plate and being temporarily flattened, but once again increasing in height because of the effects of surface tension.

Conclusion

In this article examples of simulations of a bubble column and fluidized bed have been introduced as two reactors that are most frequently discussed in chemical engineering. Moving forward, we want to develop and apply this method as an effective tool for design and rationalization of chemical processes within Sumitomo Chemical. Furthermore, multiphase flows are processes that are always seen in the fields of information processing, electronic systems, new materials and life science. We would like to develop the use of simulations for design of these apparatuses like a new tidal stream.

References

1) Kagaku Kougaku Benran (Chemical Engineering Handbook), 6th Ed., Japanese Society of Chemical Engineering, Maruzen (1999).
2) A. Tomiyama, *Proceedings of 3rd International Conference on Multiphase Flow* (CD-ROM) (1998).
3) N. Shimada, R. Saiki, A. Dhar, K. Mizuta and A. Tomiyama, *Proceedings of 1st International Symposium on Multiscale Multiphase Process Engineering* (*MMPE*) (USB), L-1 (2011).
4) T. Kobayashi, N. Shimada and T. Tanaka, *Proceedings of ASME-JSME-KSME Joint Fluids Engineering Conference 2011*, AJK2011-12011 (2011).
5) A. Dhar and N. Shimada, 77th Annual Meeting of Japanese Society of Chemical Engineering (CD-ROM), N106 (2012).
6) Suuchi Ryuutai Rikigaku Handbook (Computational Fluid Dynamics Handbook), Kobayashi T. Ed., Maruzen (2003).
7) F. Xiao, Y. Honma and T. Kono., *Int. J. Numer. Meth. Fluids*, **48**, 1025 (2005).
8) K. Yokoi, D. Vadillo, J. Hinch and I. Hutchings, *Physics of Fluids*, **21**, 072102 (2009).

PROFILE

Naoki Shimada

Sumitomo Chemical Co., Ltd.
Process & Production Technology Center
Ph.D., Researcher

Tetsuya Suzuta

Sumitomo Chemical Co., Ltd.
Process & Production Technology Center
Senior Researcher

Tomonari Kobayashi

Sumitomo Chemical Co., Ltd.
Process & Production Technology Center
Researcher